

# Active Noise Control Over Multiple Zones: Adaptive Algorithm in Time Domain

Xiaoli Tang\*, Jihui Zhang\* and Thushara D. Abhayapala\*

\*Audio & Acoustic Signal Processing, RSEEME, The Australian National University, Canberra ACT 2601, Australia  
E-mail: {Xiaoli.Tang, Jihui.Zhang, Thushara.Abhayapala}@anu.edu.au

**Abstract**—Spatial active noise control (ANC) and multizone soundfield reproduction have been active research problems that use multiple loudspeakers and multiple error microphones to control regions of interest. In this paper, we investigate the intersection of the two topics, that is multizone adaptive ANC systems. To be more specific, we derive a mathematical model based on multichannel Filtered-x Least Mean Square (FxLMS) algorithm to achieve simultaneous noise reduction over multiple regions using a single ANC system. We also build and simulate the model over two regions using two different quantities of secondary sources. The simulation results validate the theory and demonstrate the feasibility of multizone adaptive ANC.

**Index Terms**—Spatial active noise control (ANC), Multizone, Time domain processing

## I. INTRODUCTION

Spatial active noise control (ANC) is used to reduce undesired acoustic noise over a 3-D region. Listeners inside the controlled region can enjoy quiet ambience without wearing headphones. Spatial ANC is achieved using an array of loudspeakers to generate anti-noise signals to cancel them in real time [1-2]. A variety of applications such as in-car ANC [3-5] and aircraft ANC [6-7] have been active topics of research and gradually entering the market.

Apart from spatial ANC, sound reproduction over multiple regions is also a popular research area over the past years. Multizone sound control has an advantage that it enables independent and simultaneous processing over different regions in the same space [8]. The applications including simultaneous car entertainment systems and surround sound systems in exhibition centres can provide listeners specific sound environment [9]. Many approaches have been developed, such as sparse methods [10], Iterative DFT-domain Inversion [11] and orthogonal basis expansion [12].

However, even though spatial ANC and multizone sound reproduction have been well researched, so far there is limited study on the intersection of two, that is, spatial ANC over multiple regions. Recently, Zhang et al, proposed a wave-domain method that can be applied to multizone ANC for performance evaluation [13]. Chen et al, also provided an approach to evaluate the multizone noise cancellation quality inside vehicles [14]. However, the existing works focus on performance evaluation rather than adaptive solution. There is still a research gap between the theory and implementation of multizone adaptive ANC. Our research fits in this gap, and this paper aims to provide a model to achieve multizone adaptive ANC based on FxLMS algorithm [15-17].

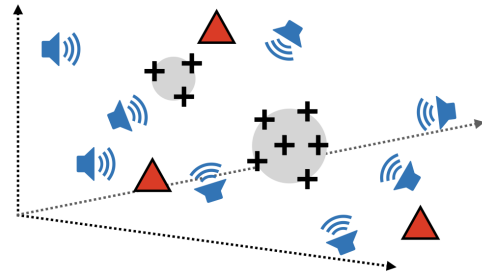


Fig. 1. General configuration of multizone adaptive ANC system in 3-D space. The grey spheres are the regions of interest, the black “+” markers on spheres indicate error microphones, the three red triangles indicate primary noise sources, and the loudspeaker symbols indicate secondary sources.

In this paper, we firstly derive the mathematical model of the ANC system over multiple regions from multichannel FxLMS algorithm. Then, we simulate the model based on the configuration of a real room. In our simulation, we control the regions using different quantities of loudspeakers. We also choose either narrowband noise or broadband noise to be the primary sources. The simulation results are given in Section IV. Finally, we evaluate the ANC performance by comparing the steady-state noise reduction (NR) level and the convergence rate of each zone.

## II. PROBLEM FORMULATION

In this section, we derive the mathematical model for the general multizone adaptive ANC system using FxLMS algorithm in time domain.

As shown in Fig. 1, in a 3-D space, let  $Z$  spherical regions with radii  $R_1, R_2, \dots, R_Z$  to be controlled. We place  $M_1, M_2, \dots, M_Z$  error microphones at the boundary of each zone based on the principle of uniform sampling [18]. Outside  $Z$  zones,  $J$  primary noise sources and  $K$  secondary sources (loudspeakers) are distributed. We model this system using feedforward control under the assumption that reference microphones are placed at the same position as the primary noise sources.

The block diagram shown in Fig. 2 demonstrates the workflow of multizone adaptive ANC system using FxLMS algorithm. The top branch presents the primary path propagation of  $J$  reference signals  $x(n)$ .  $Z$  primary-path matrices  $[P_1, P_2, \dots, P_Z]$  have dimensions  $[M_1 \times J, M_2 \times J, \dots, M_Z \times J]$  respectively.  $d_z(n)$  denotes the primary noise signals received at the  $z^{th}$  zone. Correspondingly,  $e_z(n)$  are the residual error

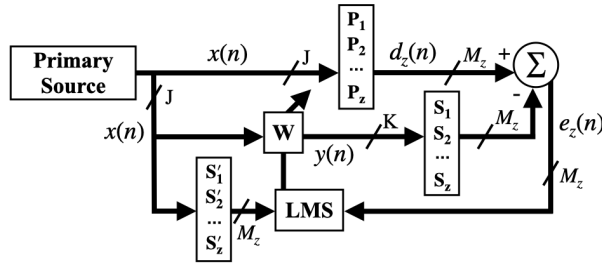


Fig. 2. Block diagram of multizone adaptive ANC system.  $x(n)$  denotes for  $J$  reference signals ( $n$  is the time step), the block  $[P_1, P_2, \dots, P_Z]$  and  $[S_1, S_2, \dots, S_Z]$  are transfer functions of the primary path and secondary path propagation for  $Z$  zones.  $[S'_1, S'_2, \dots, S'_Z]$  are secondary path estimation. The block  $W$  stands for adaptive filter.

signals of the  $z^{\text{th}}$  zone. In the following expressions, we use  $d_{z,m}(n)$  and  $e_{z,m}(n)$  to specify every single signal received at the  $m^{\text{th}}$  error microphone of the  $z^{\text{th}}$  zone. The second branch flows into an adaptive filter  $W$  ( $K \times J$ ) being updated by FxLMS algorithm. Each element of  $W$  is denoted by  $w_{kj}(n)$ . For the secondary path transfer functions  $[S_1, S_2, \dots, S_Z]$  and their estimation  $[S'_1, S'_2, \dots, S'_Z]$ , we use  $S_{z,m,k}(n)$  and  $S'_{z,m,k}(n)$  to denote every single element at an arbitrary time step  $n$ .

The residual error from the  $m^{\text{th}}$  error microphone at the  $z^{\text{th}}$  zone at time step  $n$  is given by

$$e_{z,m}(n) = d_{z,m}(n) - \sum_{k=1}^K S_{z,m,k}(n) * \sum_{j=1}^J w_{kj}^T(n) \mathbf{x}_j(n), \quad (1)$$

where  $\mathbf{w}_{kj}(n) \equiv [w_{kj,0}(n) \ w_{kj,1}(n) \ \dots \ w_{kj,L-1}(n)]^T$  with  $k = 1, 2, \dots, K$ ,  $j = 1, 2, \dots, J$ ,  $L$  is the length of filter,  $\mathbf{x}_j(n) \equiv [x_j(n) \ x_j(n-1) \ \dots \ x_j(n-L+1)]^T$ , and  $*$  stands for time-domain convolution.

We approximate the cost function of the adaptive filter by the summation of the instantaneous squared errors from all zones. To be able to control the priority of zones, we add weighting factors  $[a_1, a_2, \dots, a_Z]$  to  $Z$  zones. Then, the cost function is given by

$$\hat{\varepsilon}(n) = \sum_{z=1}^Z a_z \sum_{m=1}^{M_z} e_{z,m}^2(n). \quad (2)$$

To minimise the weighted sum of instantaneous squared error in (2), we apply the steepest descent algorithm given by

$$\mathbf{w}_{kj}(n+1) = \mathbf{w}_{kj}(n) - \frac{\mu}{2} \nabla \hat{\varepsilon}(n), \quad (3)$$

where  $\mu$  is the step size of adaption.

Then, we calculate the gradient estimate of the weighted sum of the instantaneous squared error,

$$\nabla \hat{\varepsilon}(n) = 2 \sum_{z=1}^Z a_z \sum_{m=1}^{M_z} e_{z,m}(n) [-S_{z,m,k}(n) * \mathbf{w}_{kj}^T(n) \mathbf{x}_j(n)]. \quad (4)$$

Substitute (4) into (3), we have

$$\begin{aligned} \mathbf{w}_{kj}(n+1) &= \mathbf{w}_{kj}(n) + \\ &\mu \sum_{z=1}^Z a_z \sum_{m=1}^{M_z} e_{z,m}(n) [-S_{z,m,k}(n) * \mathbf{w}_{kj}^T(n) \mathbf{x}_j(n)]. \end{aligned} \quad (5)$$

In real life, secondary path transfer functions  $S_{z,m,k}(n)$  are unknown to us. Hence, we usually use  $S'_{z,m,k}(n)$  to estimate  $S_{z,m,k}(n)$ . Then, the final update equation of the time-domain multizone algorithm can be represented as

$$\begin{aligned} \mathbf{w}_{kj}(n+1) &= \mathbf{w}_{kj}(n) + \\ &\mu \sum_{z=1}^Z a_z \sum_{m=1}^{M_z} e_{z,m}(n) [-S'_{z,m,k}(n) * \mathbf{w}_{kj}^T(n) \mathbf{x}_j(n)]. \end{aligned} \quad (6)$$

### III. SIMULATION SETUP

In this section, we present the simulation setup of multizone adaptive ANC for validation.

#### A. System Environment Setup

The system configuration is shown in Fig. 3. We conducted the simulation based on the real environment of a study room with dimensions [3.25,4.12,2.40] m. In Fig. 3 (a), the placement of two primary sources (hollow circles with black margin) corresponds to the actual positions of the electrical fan and the air-conditioner, which are at [1.54,0.12,0.50] m and [3.10,2.04,2.00] m. Two regions of interest centre at [0.92,1.50,1.54] m and [2.11,3.27,1.65] m, with the same radius of 0.04 m. We generate secondary sources using two quantities ( $K=6$  and  $K=10$ ), which are marked in red and blue crosses. The choice of two quantities is based on the total number of error microphones.  $K=10$  is considered to be adequate to achieve adaptive ANC as it is equal to the total quantity of error microphones. The system with  $K=6$  has less control, but it arouses our interest that to what extent the performance can reach. For error microphone placement, we adopt uniform sampling, i.e., at vertices of tetrahedron and octahedron inside the circumscribed spheres, and place  $M_1=4$  and  $M_2=6$  error microphones on the two spherical zones. Fig. 3 (b) shows how error microphones are placed on the boundary of zone 2.

#### B. Primary Source

We test the ANC system under two conditions - using narrowband and broadband noise as primary source signals. For each condition, two primary sources located at [1.54,0.12,0.50] m and [3.10,2.04,2.00] m generating identical signals at the same time during simulation. The narrowband noise is generated by superpositioning multiple sinusoids at low frequencies ranging from 120 Hz to 600 Hz. This is to simulate the noise from a typical electric motor or rotational machinery [19]. The broadband noise is recorded from an industrial air-conditioner [20]. Fig. 4 is the frequency spectrum of the broadband noise. The frequency range is approximately between 0 and 1 kHz, and the majority is less than 550 Hz.

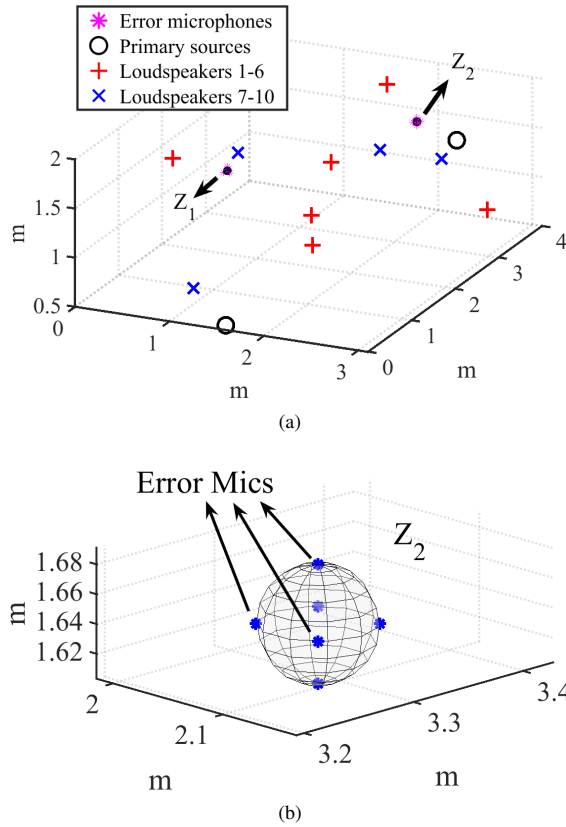


Fig. 3. (a) Simulation setup in a room with different quantities of secondary sources. Two zones are labelled with  $Z_1$  and  $Z_2$ , the two hollow circles indicate primary sources, the red '+' markers indicate loudspeakers 1-6 and the blue 'X' markers indicate loudspeakers 7-10. (b) A zoom-in view on 6 error microphones uniformly distributed on the boundary of zone 2.

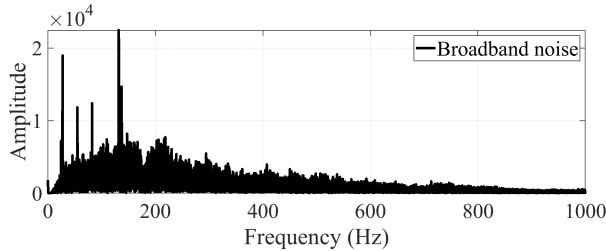


Fig. 4. The frequency spectrum of broadband noise recorded from an industrial air-conditioner.

### C. Room Impulse Response (RIR) Simulation

The image source method is utilised for room impulse response (RIR) simulation, according to the room parameters. Based on the material and surface area of the room (four concrete walls, a concrete ceiling and a carpet floor), an average reverberation time  $T_a=0.8$  seconds is calculated and applied to all surfaces of the room [21-22]. The sampling frequency of both the primary path and secondary path RIRs is set to 8 kHz.

It is worth mentioning that each path of the generated RIRs  $[S_1, S_2, \dots, S_Z]$  is at length of 4096 taps. For narrowband and broadband noise simulation, we truncate the first 500 and 1000 taps respectively to be the secondary path estimation  $[S'_1, S'_2, \dots, S'_Z]$ . The secondary path estimation is a common approach widely used in adaptive ANC systems. This estimation contains magnitude error and phase error that affects the stability of the system, and inaccurate estimation can result in system divergence [23]. In terms of our truncation, there is no estimation error in the retained portion as they overlaid the simulated taps. However, all errors come from the truncated part. Hence, we consider the truncation length as a factor affecting system stability in terms of the secondary path estimation accuracy.

### IV. SIMULATION RESULTS

In this section, the results from the simulation are presented in terms of the steady-state noise reduction (NR) and the convergence time of each zone. For an arbitrary zone  $z$  at time step  $n$ , the performance evaluation is based on total squared error  $E_z(error)$ , which is a summation of the squared error signals in the  $z^{th}$  region. The expression is given by

$$E_z(error) = \sum_{m=1}^{M_Z} e_{z,m}^2(n). \quad (7)$$

The summation of squared energy from primary noises received at each zone is given by

$$E_z(noise) = \sum_{m=1}^{M_Z} d_{z,m}^2(n). \quad (8)$$

The corresponding noise reduction in decibels (dB) is calculated from

$$NR_z(dB) = 10 \log_{10} \frac{E_z(error)}{E_z(noise)}. \quad (9)$$

We show the ANC performance of narrowband noise on  $K=10$ , and broadband noise on both  $K=10$  and  $K=6$  in the following subsections.

#### A. Narrowband Noise as Primary Source

In Fig. 5, the curves in the (a), (b) are NR of two zones over 1440 seconds. The simulation time is set longer to ensure the average NR curves are fully flattened. However, the actual convergence time is not that long, but at the very beginning of the simulation. Fig. 5 (c), (d) present zoom-in views on the convergence of  $E_z(error)$  at each zone. The energy of error signals of both zones drops quickly and reach steady-state within 10 seconds. The maximum NR is approximately -25.2 dB for zone 1 and -30.1 dB for zone 2.

#### B. Broadband Noise as Primary Source

Apart from the narrowband noise, we also investigate the broadband noise performance. The simulation results from  $K=10$  and  $K=6$  presented in Fig. 6 (a) and (b) show the average NR for each zone using two quantities of the loudspeaker. In both configurations, the overall noise has been reduced by

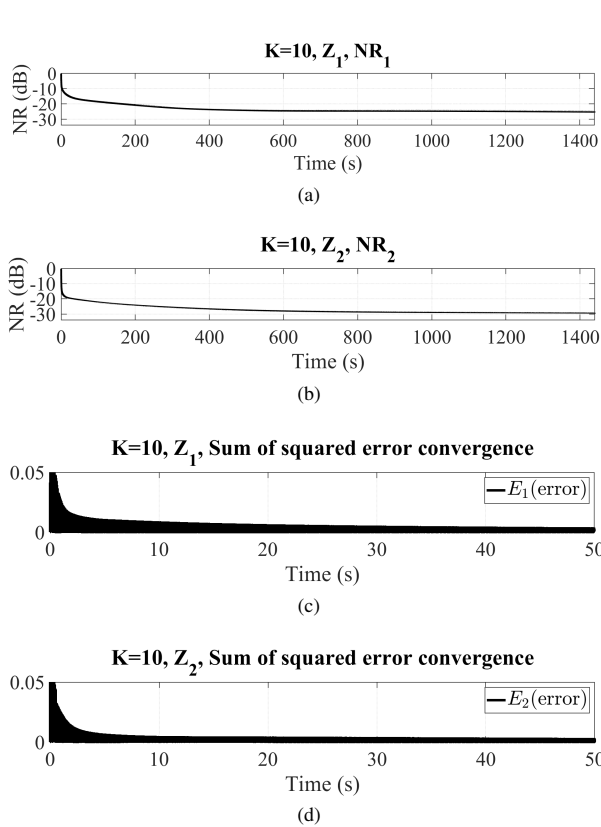


Fig. 5. The NR curves and the zoom-in view of squared sum of energy convergence of dual-zone (equally weighted) ANC with  $K=10$  under narrowband noise. (a) NR in decibel of zone 1, (b) NR in decibel of zone 2, (c) zoom-in view of convergence on  $E_1(error)$ , (d) zoom-in view of convergence on  $E_2(error)$ .

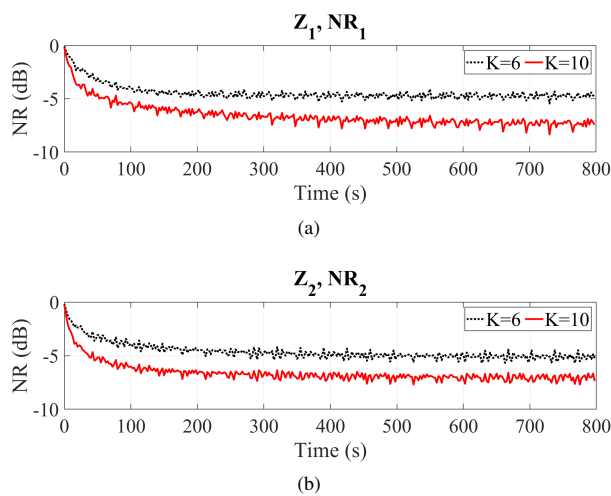


Fig. 6. The NR curves of dual-zone (equally weighted) ANC with  $K=10$  and  $K=6$  under broadband noise. (a) NR in decibel of zone 1, (b) NR in decibel of zone 2.

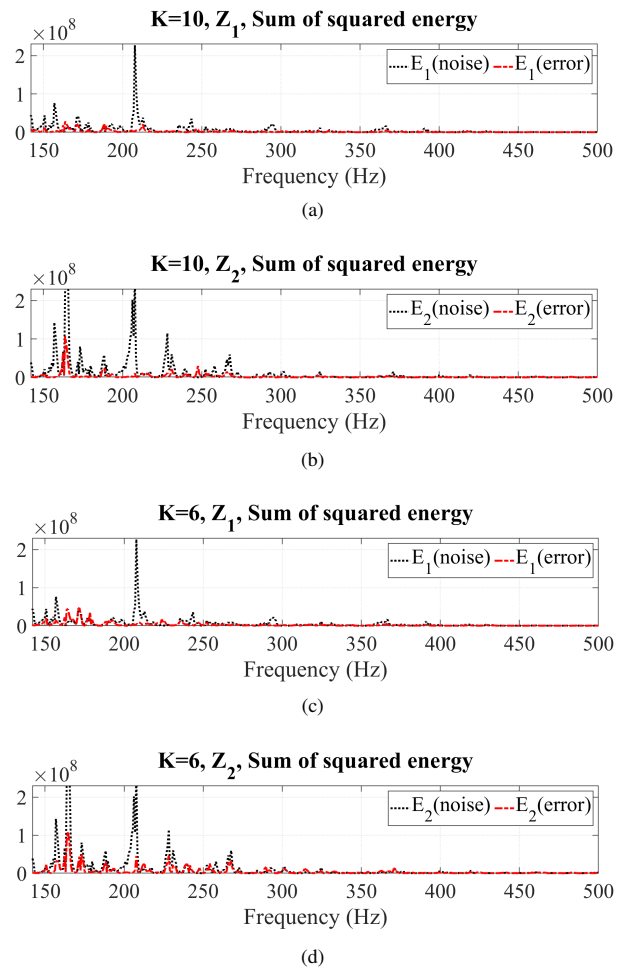


Fig. 7. The total squared energy versus frequency of dual-zone (equally weighted) ANC with  $K=10$  and  $K=6$  under broadband noise. (a), (c) Total squared energy of noise and error of zone 1, (b), (d) total squared energy of noise and error of zone 2.

more than half (-3 dB) within a minute in each zone. The convergence time are similar at approximately 300 seconds, except for zone 1 with  $K=10$ . At the end of simulation, the NR difference between  $K=10$  and  $K=6$  is around 2 to 3 dB, showing that better performance is achieved with more loudspeakers. For broadband noise, the overall performance is inferior to narrowband noise due to the wider bandwidth and the time-varying frequencies.

The accuracy of the image source method is influenced by geometry as it is based on geometrical-acoustic (GA) modelling technique [24]. In specific, the longest valid wavelength of sound in the simulation should be less than all geometry details. According to this limitation, in our setup, simulation results for frequencies below 143 Hz are inaccurate, so we mainly investigate the frequencies above it. Fig. 7 presents the  $E_z(noise)$  and  $E_z(error)$  in frequency domain at the end of simulation (800 seconds). The most peaks of noise energy are reduced in both zones using either quantity of loudspeakers.

We also found that giving weight to each zone can balance the performance between them. For example, adding more weight to the zone with less NR will result in better performance. However, in the meantime, weights on other zones could drop and lead to less control.

#### V. CONCLUSION

In this paper, we proposed a mathematical model of time-domain FxLMS along with its derivation to achieve adaptive ANC over multiple regions using a single system. We also validated this approach through simulation on narrowband noise and broadband noise and using two quantities of the secondary source.

The simulation results demonstrated the feasibility of simultaneous multizone adaptive ANC. We found that the performance in terms of the steady-state NR and the convergence time can be improved by increasing the number of loudspeakers. Adding weight to a particular zone also enhances its performance.

Multizone adaptive ANC can be used when we need to create multiple quiet areas in a shared place, such as office, library, or residential community, with a single ANC system. The priority of the controlled regions can also be adjusted according to different situation.

Future works can be implementing multizone adaptive ANC system in frequency domain and conducting experiments.

#### REFERENCES

- [1] S. M. Kuo and D. R. Morgan, "Active noise control: a tutorial review," *Proceedings of the IEEE*, vol. 87, no. 6, pp. 943-973, 1999.
- [2] J. Zhang, "Active Noise Control Over Spatial Regions," PhD, Australian National University, Canberra, 2019.
- [3] P. N. Samarasinghe, W. Zhang, and T. D. Abhayapala, "Recent advances in active noise control inside automobile cabins: Toward quieter cars," *IEEE Signal Processing Magazine*, vol. 33, no. 6, pp. 61-73, 2016.
- [4] H. Chen, P. Samarasinghe, T. D. Abhayapala, and W. Zhang, "Spatial noise cancellation inside cars: Performance analysis and experimental results," in *2015 IEEE Workshop on Applications of Signal Processing to Audio and Acoustics (WASPAA)*, 2015: IEEE, pp. 1-5.
- [5] H. Sano, T. Inoue, A. Takahashi, K. Terai, and Y. Nakamura, "Active control system for low-frequency road noise combined with an audio system," *IEEE Transactions on Speech and Audio Processing*, vol. 9, no. 7, pp. 755-763, 2001.
- [6] D. Miljković, "Active noise control in light aircraft cabin using multi-channel coherent method," *Automatika*, vol. 57, no. 4, pp. 1056-1069, 2016.
- [7] O. Pabst, T. Kletschkowski, and D. Sachau, "Active noise control in light jet aircraft," *Journal of The Acoustical Society of America*, vol. 123, no. 5, pp. 3875-3875, 2008.
- [8] W. Zhang, T. D. Abhayapala, T. Betlehem, and F. M. Fazi, "Analysis and control of multi-zone sound field reproduction using modal-domain approach," *The Journal of the Acoustical Society of America*, vol. 140, no. 3, pp. 2134-2144, 2016.
- [9] Y. J. Wu and T. D. Abhayapala, "Spatial multizone soundfield reproduction: Theory and design," *IEEE Transactions on Audio, Speech, and Language Processing*, vol. 19, no. 6, pp. 1711-1720, 2010.
- [10] W. Jin and W. B. Kleijn, "Theory and design of multizone soundfield reproduction using sparse methods," *IEEE/ACM Transactions on Audio, Speech, and Language Processing*, vol. 23, no. 12, pp. 2343-2355, 2015.
- [11] M. Buerger, C. Hofmann, C. Frankenbach, and W. Kellermann, "Multizone sound reproduction in reverberant environments using an iterative least-squares filter design method with a spatiotemporal weighting function," in *2017 IEEE Workshop on Applications of Signal Processing to Audio and Acoustics (WASPAA)*, 2017: IEEE, pp. 1-5.
- [12] W. Jin, W. B. Kleijn, and D. Virette, "Multizone soundfield reproduction using orthogonal basis expansion," in *2013 IEEE International Conference on Acoustics, Speech and Signal Processing*, 2013: IEEE, pp. 311-315.
- [13] J. Zhang, H. Sun, P. N. Samarasinghe, and T. D. Abhayapala, "Active Noise Control Over Multiple Regions: Performance Analysis," in *ICASSP 2020-2020 IEEE International Conference on Acoustics, Speech and Signal Processing (ICASSP)*, 2020: IEEE, pp. 8409-8413.
- [14] H. Chen, P. Samarasinghe, and T. D. Abhayapala, "In-car noise field analysis and multi-zone noise cancellation quality estimation," in *2015 Asia-Pacific Signal and Information Processing Association Annual Summit and Conference (APSIPA)*, 2015: IEEE, pp. 773-778.
- [15] I. T. Ardekani and W. H. Abdulla, "FxLMS-based active noise control: a quick review," in *Proceedings of 2011 Asia Pacific Signal and Information Processing Association Annual (APSIPA) Summit and Conference*, 2011, vol. 1, pp. 1-11.
- [16] X. Tang and C.-M. Lee, "Time-frequency-domain filtered-x LMS algorithm for active noise control," *Journal of Sound and Vibration*, vol. 331, no. 23, pp. 5002-5011, 2012.
- [17] E. Bjarnason, "Analysis of the filtered-x LMS algorithm," *IEEE Transactions on Audio, Speech, and Language Processing*, vol. 3, no. 6, pp. 504-514, 1995.
- [18] B. Rafaely, *Fundamentals of Spherical Array Processing*. Springer, 2015.
- [19] Matlab. "Active Noise Control Using a Filtered-X LMS FIR Adaptive Filter." <https://www.mathworks.com/help/audio/examples/active-noise-control-using-a-filtered-x-lms-fir-adaptive-filter.html> (accessed May, 2020).
- [20] E. Sound. "Make your content come to life with our sound effects." <https://www.epidemicsound.com/sound-effects/> (accessed April, 2020).
- [21] H. Kuttruff, *Room Acoustics, Fifth Edition*. Taylor & Francis, 2009.
- [22] E. Toolbox. "Room Sound Absorption - Sound Absorption Coefficient." [https://www.engineeringtoolbox.com/acoustic-sound-absorption-d\\_68.html](https://www.engineeringtoolbox.com/acoustic-sound-absorption-d_68.html) (accessed June, 2020).
- [23] C. Hansen, S. Snyder, X. Qiu, L. Brooks, and D. Moreau, *Active Control of Noise and Vibration*. CRC press, 2012.
- [24] L. Savioja and U. P. Svensson, "Overview of geometrical room acoustic modeling techniques," *The Journal of the Acoustical Society of America*, vol. 138, no. 2, pp. 708-730, 2015.